THE DIURNAL CYCLE OVER LAND

Alan K. Betts

Atmospheric Research, Pittsford, Vermont 05763

akbetts@aol.com

[Betts, A.K., 2003: The diurnal cycle over land. Chapter 6, pp. 73-93, of *"Forests at the Land-Atmosphere interface"* ISBN: 0851996779, 304pp, Eds., M Mencuccini, J Grace, J Moncrieff and K. McNaughton, publisher CABI Publishing, Wallingford, Oxon OX10 8DE, UK.]

1. INTRODUCTION

This paper reviews, initially from an observational perspective, the nature of the diurnal cycle over land, using illustrations from high latitudes to the tropics. Understanding the coupling between different processes at the land surface is of fundamental importance, because in global models, many processes are parameterized, and are poorly constrained by routine observational inputs. Yet the diurnal cycle is observed synoptically, so it is an excellent indicator of whether the surface processes and their interaction with the boundary layer (BL) are modeled correctly. In addition, the diurnal range of surface temperature and humidity are important prognostic variables for society.

First some basic concepts are reviewed, with illustrative examples, and then additional controls on the diurnal cycle at high latitudes are discussed. Finally a tropical example (over Rôndonia in the southern Amazon basin) will be used to illustrate the difficulty in getting the diurnal cycle of precipitation right in a forecast model, because of the interaction of many processes.

Near the earth's surface, the incoming solar radiation drives a characteristic diurnal cycle for many variables. The atmosphere is relatively transparent to the short-wave radiation from the sun and

relatively opaque to the thermal radiation from the earth. As a result, the surface is warmed by a positive net radiation balance in the daytime, and cooled by a negative radiation balance at night. The surface temperature oscillates between a minimum at sunrise and a maximum in the afternoon. In warm seasons, the daily net radiation balance is positive, and the daily mean temperature is determined by the daily mean surface energy balance, which involves not only the short and long-wave radiation components, but also heat transfers to the atmosphere. The magnitude of this diurnal range of temperature is determined by many factors. The most important are the nature of the underlying surface, whether land or water, and the coupling to the atmosphere above. The phase change of water, particularly evaporation and condensation plays an important role in moderating the diurnal range of temperature, because of the large latent heat of vaporization. (In cold climates the freezing and thawing of the soil is also important on the seasonal timescale.)

Over the ocean (and large lakes), the diurnal temperature range is small, because the incoming solar energy is mixed downward into an ocean “mixed layer”, which is usually tens of meters deep. One day of solar heating will warm a layer of water 50m deep less than 0.1K, because of its large thermal capacity. Only in light winds, when the downward mixing is small, does the diurnal range of sea surface temperature reach 1K. On time-scales longer than the diurnal, evaporation of water primarily balances the surface net radiation budget.

Over land, only a small fraction (<20%) of the net radiation at the surface is conducted downward in the daytime, stored by warming trees on the surface, or partly used for photosynthesis. As a result, the surface temperature rises rapidly after sunrise, until near-balance is achieved between the net radiation and the direct transport of heat to the atmosphere (referred to as the sensible heat flux) and evaporation of water (or transpiration from plants), referred to as the latent heat flux. If the surface

is a desert, then the daytime temperature rise is large, but if water is readily available for transpiration, the daytime rise of temperature is greatly reduced, because most of the net radiation goes into the latent heat of vaporization. The surface sensible and latent heat fluxes have a large diurnal cycle, with a peak near local noon, as they are driven primarily by the incoming solar radiation. The surface temperature peaks a little later in the afternoon, and the surface sensible heat flux goes negative once the surface cools sufficiently. The challenge in a numerical model is to get the surface net radiation correct (which depends on the cloud field, as well as the atmospheric structure and aerosols), and predict the correct evaporation, which is constrained over land by vegetative and soil thermal and hydrologic processes (which in turn depend on the model precipitation).

2. ILLUSTRATIVE EXAMPLES

2.1 Dependence of diurnal cycle on evaporation

Figure 1 illustrates this diurnal variation using data from sunny days in mid-summer during a 1987 field experiment (the First International Satellite Land-surface Climatology Project Field Experiment, FIFE) conducted over grassland near Manhattan, Kansas. The panels on the left show from top to bottom, net radiation, R_n, sensible heat flux, H, and latent heat flux, LE (data from Betts and Ball, 1995). The surface energy balance can be written as

$$R_n = H + LE + G \qquad (1)$$

where G is the storage in the ground and vegetation, which we do not show. In addition a small amount of energy goes into photosynthesis, which again we do not show. The time axis is local solar time, which is UTC-6 hours. The data have been grouped and averaged based on the percent soil moisture (SM) in the first 10cm of soil, so that there are three curves (each an average of about 10 days) representing dry, medium and wet soils. The upper left panel shows that the mean net radiation on these sunny days is very similar. However because soil moisture is a major control on evaporation, the partition of the net radiation into sensible and latent heat is very different. When the soil is wet, the latent heat flux (or "evaporative energy" flux) is about three times the sensible heat flux, whereas when the soil is dry, these two fluxes are nearly equal. The panels on the right side show the response to the different surface forcing. The upper right panel shows the surface temperature (measured by an infrared radiation thermometer, mounted on a tower and pointed downward at the grass). Although R_n is almost the same in all composites, on days when the soil is dry and water is not readily available for evaporation, the surface gets very hot, as warm as 44^{o}C near noon. This warm surface temperature drives the large sensible heat flux H and heats the air above the surface. The diurnal range of the surface temperature is more than 20^{o}C on these days, while for the air at 2m above the surface in the middle panel, the diurnal range is only 12^{o}C. As soil moisture increases, the daily maximum surface and air temperature decrease. The upper two panels on the right are similar, except that the amplitude of the surface temperature is larger than that of the air temperature. The difference is related to the sensible heat flux H. Note that the air temperature has a broad afternoon maximum, because H is upward as long as the surface is warmer than the air. The surface temperature falls below the air temperature only in late afternoon, H then changes sign, and at night the surface is cooler than the air. The lower right panel shows the diurnal cycle of relative

humidity (RH) as a percent. Over the wetter soils, the RH of the air at 2m reaches 85% before sunrise, and falls in the daytime as the surface and air warms. The fall of RH is smallest on the days with the greatest evaporation, LE. When evaporation is reduced because the soil is dry, daytime RH falls as low as 30%, and even at night only reaches 72% at sunrise.

2.2 Coupling between the surface diurnal cycle and the atmospheric mixed layer

As the land surface is heated during the daytime, a dry convective boundary layer grows in depth. This is called the "mixed layer", because the turbulent dry convection rapidly stirs the layer to one of near-neutral buoyancy and near-constant water vapor mixing ratio. The diurnal cycle of the surface and the mixed layer are tightly coupled. As a result the preexisting atmospheric structure above the surface at sunrise has a considerable impact on the daytime diurnal cycle, as illustrated in the following figures using surface and sounding data collected over the boreal forest in Saskatchewan, Canada during the Boreal Ecosystem-Atmosphere Study (BOREAS) in 1994. Figure 2 shows the surface diurnal cycle for two days in spring. The upper panel shows for each day the temperature at two levels, an upper level (T_U) which is at 21m, about 5m above the canopy of a jack-pine forest, and a lower level (T_L) about 5m above the forest floor. On both days the surface cools strongly at night and rises steeply after sunrise with a greater diurnal range than in Figure 1. The diurnal range under the canopy is larger than above it. At night on May 26, the winds are lighter, and the atmosphere above is more stable (see later figure). The air under the canopy becomes effectively decoupled from the atmosphere above and the stable temperature gradient across the canopy at night reaches 7K. There is very little evaporation from either the forest, or the cold lakes at this time in

spring. The lower panel shows RH measurements above the canopy. In the late afternoon, RH falls as low as 20% on May 31. Before sunrise on this day, RH above the canopy reaches 90% as T_U falls to a minimum of 4°C. RH was not measured below the canopy, but the temperatures there are cold enough to saturate the air in the hours before sunrise. The dew point is often used to estimate minimum night time temperatures at the surface.

The right hand scale of the upper panel shows the corresponding dry potential temperature, which is defined as

$$\theta = (T+273.15)(1000/p)^{0.286} \quad (2)$$

where p is the surface pressure (here about 950 hPa, since the observation site is about 500m above sea level). The potential temperature, θ, is useful as a variable because it allows us to compare surface and atmosphere above. During the daytime the boundary layer above the surface is mixed to almost constant potential temperature (see Figure 3). The strong radiative cooling of the surface at night generates a stable layer close to the ground, typically only a few hundred meters deep. About three to four hours after sunrise, the surface has warmed enough to remove this stable surface layer and reconnect to a deeper layer. When this happens, the rate of rise of temperature and fall of RH decrease sharply. In Figure 2, this occurs on May 26 at a local time of 8.8 h, when θ reaches 296K; while on May 31, it occurs at 7.8 h, when θ= 289K, and on this day the change is smaller. Figure 3 shows sequences of seven profiles of potential temperature in the lower troposphere, measured by rawinsonde ascents, nominally every 2 hours from sunrise to late afternoon on the two days. The upper panel shows at sunrise (0417 LST, light solid) a cold (stable) surface layer only about 25 hPa deep (200m), with a deep layer above of constant θ, which is the residual or “fossil” mixed layer from the previous day. At the surface the temperature warms rapidly, as the surface

sensible heat flux is trapped in this shallow surface layer. The profile at 0824 LST shows a mixed layer with θ= 294.5K to 890 hPa. Shortly afterwards, when the surface potential temperature reaches θ= 296K, the new growing boundary layer merges with the deep residual mixed layer. From then on, the surface and mixed layer warm much more slowly, as seen in Figure 2. Even though H exceeds 300 Wm^{-2} at all the forest sites for several hours around local noon (not shown), this large heat flux is distributed through a deep layer.

The lower panel shows the time-sequence on May 31. Note that at sunrise, the profile is quite different than on May 26. Instead of a deep layer of constant θ, produced by dry convection the previous day (a so-called dry adiabatic structure), there is a layer from 920 to 650 hPa in which θ increases steadily with height. In fact this layer was produced by showers the previous evening (and it has a wet adiabatic structure). The change in slope of the early morning profile at 920 hPa is at θ= 289K, and hence we see on Figure 2 a change in the rate of warming, once the surface reaches this potential temperature. This change of slope is more dramatic on May 26, because the change in the vertical profile is also greater. On May 31, the mixed layer grows steadily all day until it is 300 hPa deep (about 3000m) in the late afternoon. On both these days, there is some broken cumulus cover in the afternoon at the top of the mixed layer. The rapid warming on May 31, that is seen between 500 and 600 hPa, is related to the lowering and change in structure of a powerful jet-stream above, not by surface processes.

2.3 Fundamental relationship between relative humidity (RH), saturation pressure, and cloud-base

Many introductory courses in meteorology imply that RH is not a fundamental variable. Rather

mixing ratio, a conserved quantity, is presented as a more basic variable. However, there are many parameters conserved in different processes in the atmosphere, and each tells its own story. RH does has a fundamental significance, because of its tight relationship to saturation pressure (which is conserved in dry and wet adiabatic processes: Betts, 1982), and hence to lifting condensation level (LCL) and cloudbase (the critical level of the liquid phase transition, which affects radiative and microphysical processes). However, this link is generally poorly appreciated, and consequently the value of saturation pressure in modeling has not been fully explored. [Another unfortunate byproduct perhaps is that RH has not traditionally been measured at climate stations]. This link is critical over land because the availability of water for evaporation is a major control (together of course with advection) on mixed layer RH, and hence cloud-base, and this relationship is largely independent of temperature. Figure 4a shows the relation between height of the LCL and RH as surface temperature varies, and Figure 4b the corresponding relationship with $P_{LCL} = p_0 - p^*$ the pressure height to the saturation level, p^*, or LCL. It is useful to keep in mind some characteristic values. Over the ocean, as is well known, typical cloud-base height of 500m or $P_{LCL} \approx 50$hPa, corresponds to RH≈80%. Over Amazonia in the rainy season, afternoon cloudbase may reach (in some wind regimes: Betts *et al*., 2002) around 800m, or $P_{LCL} \approx 80$ hPa with RH≈70%. Over the boreal forest in spring, as in the previous section, cloudbase may reach around 2500m, or $P_{LCL} \approx 200$ hPa with RH≈30%; while over a desert, where water is largely unavailable for evaporation, cloudbase may be 3500m, $P_{LCL} \approx 300$ hPa with RH≈20% (or less).

Formally P_{LCL} is directly related to (1-RH) by the formula (Betts, 1997)

$$P_{LCL} = p(1-RH)/(A+(A-1)RH) \qquad (3)$$

where $A = (0.622\, L/2\, C_p T)$ increases with decreasing temperature from 2.6 at 25°C to 3.4 at -40°C,

with L the latent heat of vaporization and C_p the specific heat of air at constant pressure.

2.4 Link between soil water (and resistance to evaporation) and P_{LCL}

Figure 5 shows how soil water, which is a primary control on "resistance to evaporation" over land, controls the diurnal cycle of LCL (and RH.). Figure 5a is the mean diurnal cycle of P_{LCL} from ERA-15 (the European Centre 15-year reanalysis) averaged for nine Julys over the Missouri river basin (from *Betts*, 2000), and binned by soilwater in the first model layer below ground (0-7cm). There is a monotonic shift of the diurnal cycle of P_{LCL}, and an increase in its amplitude for drier soils. RH goes down and LCL (related to cloud-base) goes up as the resistance to evaporation at the surface, controlled by soilwater, decreases. (The model resistance actually depends on the whole root zone soil water with bounds at the permanent wilting point of 0.131, and the field capacity of 0.323). Figure 5b, for composites for the two summers of 1987 and 1988 from FIFE (1987 was shown in Figure 1), shows that the data shows a similar behaviour, although rather less pronounced than the model.

2.5 Diurnal cycle of CO_2

As we move towards fully coupled earth system models, capable of simulating the changing climate of the earth, the coupling of CO_2 with the meteorological and climate fields is a critical issue. The diurnal cycle of the solar radiation drives a diurnal cycle in CO_2 through photosynthesis and respiration in plants. Respiration depends strongly on temperature, and at high latitudes the seasonal

cycle of the diuranl cycle is large. Figure 6 shows the mean diurnal cycle over a young jack pine canopy (about 5-6m tall) near Thompson, Manitoba from the 1996 BOREAS experiment for three months, June, August and October (from Betts *et al.*, 2001). During the summer months, CO_2 decreases during the daylight hours as it is taken up in photosynthesis, and increases at night as it is released by respiration from both plants and soil. The amplitude of the diurnal cycle increases from June to August, as both photosynthesis and respiration increase, but the monthly mean decreases as there is a net CO_2 uptake by the entire northern hemisphere. By October of this year, however, the diurnal cycle is very small, as temperatures have dropped low enough that both photosynthesis and respiration have almost ceased. The next generation of forecast models, which assimilate CO_2 data need to get this diurnal cycle correct at the surface and in the BL. Evaporation and photosynthesis are tightly coupled, and consequently, there is a tight coupling between CO_2 and water vapour in the BL.

2.6 Coupling of water vapour and CO_2 within the BL.

During the growing season, water vapour and CO_2 gradients are strongly coupled through the daytime convective BL. Figure 7a shows the high correlation between BL fluctuations of mixing ratio, q, and CO_2, as air is mixed between the surface, where q is high and CO_2 low, and the free troposphere, where q is low and CO_2 is relatively high. The data is from the Canadian Twin Otter research aircraft (MacPherson, 1994). Figure 7b shows that the gradient on a (q, CO_2) plot within the BL is similar on different days near local noon (1830 UTC), and is presumably controlled by stomatal transpiration and uptake of CO_2.

3. THE BOREAL FOREST

An illustration from the boreal forest was used in Figure 2 to show the coupling of the diurnal cycle to the residual BL. Here two other aspects are shown: the seasonal cycle of the diurnal cycle, and the dependence of the diurnal cycle of P_{LCL} on surface water.

3.1 Seasonal cycle of diurnal cycle at high latitudes.

The freezing and thawing of the soil plays an important role in the climate at high latitudes. Winter temperatures are moderated by two processes. The first is the role of the snowpack as an insulator of the soil. The second is the freeze process, which increases the effective heat capacity of the soil by a factor of 20 (Viterbo *et al.*, 1999). This freeze-thaw introduces a significant lag into the climate system. In spring, a significant part of the net radiation goes into melting the snowpack, thawing the ground (Rouse, 2000), and melting the lakes (and in warming them). This energy becomes available in fall and the early winter, when the surface refreezes. In spring also the ground thaw, which occurs when daytime temperatures rise well above freezing, is the key control on surface evaporation. Water is not available for transpiration in spring until the snow melts and the ground thaws, and for evaporation until the ground, wetlands and lakes warm with respect to the atmosphere. Jarvis and Linder (2000) suggest that it is the snowmelt that first introduces liquid water into the soil profile. This unavailability of liquid water leads to very low evaporative fractions in spring, with large sensible heat fluxes off the forest canopy, which in turn produce deep dry BLs in spring (as in Fig.

3). In fall, when the lakes and ground are warm relative to the cooling atmosphere, the situation reverses. Evaporative fraction is high for the conifers and lakes (but not for the deciduous species after leaf fall). Net radiation is much lower by the time the surface freezes, so sensible heat fluxes are very low, and boundary layers in fall become very shallow, often capped by stratocumulus.

These seasonal changes in BL depth are very clear in graphs of P_{LCL} . Figure 8a (from Betts *et al*., 2001) shows the mean diurnal cycle of temperature (averaged for the 3 years 1994-1996) from April (month 4) to October (month 10) for a site near Thompson, Manitoba (-97.92 W, 55.80 N, elevation 221m). The peak daytime temperatures are barely above freezing in April and rise rapidly to a maximum in July and August, before falling again. In October, when the Sun angle is low, the mean diurnal cycle is small and near freezing again. Figure 8b shows the seasonal trend of P_{LCL} for Thompson. P_{LCL} falls (and RH rises) almost monotonically from April to October both during the day and at night. Conditions are so dry in Spring, because the ground is still frozen and water is not available for evaporation. Because the trees have strong stomatal control, they can survive with high canopy temperatures (20-30^{o}C), while their roots are still frozen. The particularly sharp fall from September to October is probably not just a local effect, but associated in part with the systematic advection of shallow BLs from the north.

3.2 Dependence of P_{LCL} on surface water availability.

This site near Thompson has a stand of mixed spruce and poplar with a thick surface cover of moss. This acts as a reservoir for surface water, which has a large impact on evaporation, which falls on sequential days following significant rainfall events (>5mm). This impact can be seen in Figure

9 on the diurnal cycle of P_{LCL} stratified by a wet surface index (see Betts *et al*., 1999, 2001). In this composite of all days from May to September, 1994-1996, WS=0 represents days when the moss has dried out (negligible rain for 5 days), and WS = 5 represents days when $\geq$5mm of rain fell the preceding day. The diurnal cycle depends strongly on the availability of water for evaporation at the surface (in part because evaporation from the conifers is subject to tight stomatal control). Within a few days following large rain events, mean afternoon cloud-base height rises dramatically as the surface dries out, until the characteristic deep dry BLs over the summer boreal forest are again established.

4. DIURNAL CYCLE IN RONDÔNIA IN RAINY SEASON

In this section model output from the European Centre for Medium-range Weather Forecasts (ECMWF) is compared with data collected at a pasture site located near Ouro Preto d'Oeste, Rondônia, Brazil (10.75^{o}S, 62.37^{o}W; about 30 km northwest of Ji-Parana) during the wet season months of January and February 1999 as part of the LBA (Large-scale Biosphere-Atmosphere Experiment in Amazonia) wet season campaign. The site is part of a large deforested area (> 250 km^2) dominated by a short grass with isolated palm and hardwood trees scattered throughout the landscape. At this site a micromet tower, eddy correlation instrumentation and a gas analyzer measured the surface meteorology and energy balance components. For the comparison here we use hourly averaged data from the analysis of Betts *et al*. (2002). The ECMWF model outputs (for the nearest model gridpoint) used for comparison were from 12-36 hour short range forecasts, run at a triangular truncation of T319 and a vertical resolution of 60 levels, from each operational 1200 UTC

analysis. The forecast model was the operational ECMWF model in Fall 2000, which includes the tiled land surface scheme (with acronym TESSEL, Van den Hurk *et al*., 2000), and recent revisions to the convection, radiation and cloud schemes described in Gregory *et al*. (2000). The purpose of this section is to illustrate how timeseries data from a field experiment can be used to check model output timeseries, and identify where and why a model fails to represent properly the observed atmospheric processes. This is critical research, as there remains a significant gap between real observable atmospheric processes, and our ability to represent them parametrically in numerical models, and this limits our confidence in for example climate simulations.

4.1 Composites by lower tropospheric wind regime.

Composites are useful for the comparison between model and surface observations as they average over several days and the individual small scale convective events within them, and give a picture of the mean diurnal cycle, more representative perhaps of the 60x60km grid square used in this global forecast model. We group the 40 days (from Day of Year 20 to 59) for which we have data at the pasture site, into the five groups shown in Table 1. The first four correspond to the surface easterly and westerly lower tropospheric wind regimes in the analysis of Rickenbach *et al*. (2002). These two distinctly different lower tropospheric wind regimes in Rondônia were associated with significant differences in convection. Typically, the westerly regime was associated with a moister troposphere, and convection with weak vertical development and weak electrification, while the easterly regime had a slightly drier troposphere, stronger electrified convection with greater vertical development. The fifth group in Table 1 is a composite of eight selected days, when a strong rain-

band passed directly over the measurement site in the mid-afternoon. This is shown as a separate group, since strong convective downdrafts in the afternoon produce such a distinct modification to the diurnal cycle, in order to see whether this feature is reproduced in the model. The last two columns compare the mean daily observed and model precipitation. Daily "observed" precipitation was defined by first taking the mean of the rain gages in four networks (established to validate the Tropical Rainfall Measuring Mission satellite: TRMM), and then averaging these four means (see Betts *et al*., 2002). This basic grouping by the sequence of lower tropospheric easterly and westerly components also represents a time progression of the rainy season.

For the entire 40-day period (last row), the mean daily precipitation for the TRMM raingage networks is 7.4mm, in close agreement with the model's 7.6 mm. However the model does not reproduce well the increasing temporal trend of precipitation of the first four composites, and on a daily basis the correlation between model and raingage observations is poor (not shown).

4.2 Diurnal cycle of precipitation

Despite reasonable agreement in mean precipitation during the rainy season, the current ECMWF model has a clear error in its diurnal cycle of precipitation over Rondônia, as shown in Figure 10. The composites reflect the five groups of days in Table 1. On the left is the current ECMWF model using TESSEL as its land surface model and a CAPE convective closure for deep convection (Gregory *et al*., 2000). Every model composite has a rainfall peak just after 1200 UTC, about 2 hours after sunrise, which is not observed in any of the composites on the right, derived from an average of four TRMM rain-gage network networks in Rondônia. Most days have afternoon rainfall

maxima, some have rain also at night, while all have a rainfall minimum in the morning for the period 1200-1400 UTC [0800-1000 LST]. This is also the time when the TRMM radars shown a minimum in both fractional rain area and conditional rain intensity (Rickenbach *et al*., 2002). We will discuss in section 4.4 the reasons why the model convective parameterizations produce a precipitation maximum in the morning at a time when in reality rainfall is a minimum. The model produces a secondary rainfall maximum in late afternoon. For the WET-8 rainband composite, this peak is slightly higher than for the other composites, consistent with the observations (although the model peak is later in time and broader). For the last westerly composite (53-59), the model is consistent with the data in having a weaker diurnal cycle of precipitation, including more precipitation at night.

4.3 Comparison of surface thermodynamic cycle.

Figure 11 compares the mean surface thermodynamic cycles of potential temperature, θ, mixing ratio, q, equivalent potential temperature, θ_E, and pressure height to the lifting condensation level, P_{LCL}, between the ECMWF model on the left and the pasture site observations on the right. Overall the model biases are rather small, typically cooler and wetter in the daytime. As a result the model has a lower mean P_{LCL}, corresponding to a lower mean cloud-base, and rather little bias in mean θ_E. In the model, the earlier onset of precipitation in the diurnal cycle is producing a cooler and moister BL in the daytime by the evaporation of falling precipitation. A distinct break in the model diurnal cycle can be seen, particularly in q and θ_E profiles, at 1200 UTC with the onset of rain. Unlike the data, the model shows little variability in maximum temperature. The model does show some

differences in q structure between easterly and westerly wind regimes (although the convective parameterizations are not directly aware of wind shear). The easterly regimes are wetter, with a higher afternoon θ_E, then the westerly regimes, and do not show a morning fall of q. However this is not in agreement with the observations, which show the morning fall of q for the easterly regime, and mean q increasing from beginning to end of the period (consistent with the mean precipitation increase). The θ_E comparison of the WET-8 rainband composite shows that the model does not represent the unsaturated downdraft process, which brings low θ_E air down to the surface. Unlike the downward spike in the data at the time of the rainfall maximum, the model has a θ_E maximum at the time of its rainfall maximum, which is later at 2000 UTC. The P_{LCL} comparison shows a much larger variation in the data, with the model resembling most closely the low cloud-base case of the last westerly regime, which has more frequent weaker showers and the weakest diurnal cycle of rainfall. It is clear that the mechanisms by which the model convective parameterizations for shallow and deep convection are producing precipitation and modifying the BL, while they produce a plausible diurnal cycle of cloud-base and θ_E, do not reproduce in detail the variability observed over Rondônia in these composites. The morning onset of precipitation is too early, which truncates the growth of the shallow cumulus BL, and the unsaturated downdraft process seems largely missing. It seems likely that improving the diurnal evolution of the CBL, so that the morning transition to deep convection is delayed, may significantly improve the model over land in the tropics.

4.4 Discussion of this model diurnal cycle error.

The purpose of these comparisons was to understand in more detail (and then correct) the error in

the diurnal cycle of precipitation seen in Figure 10. Some progress has been made in understanding the early onset of precipitation in the model. The diurnal evolution of the tropical BL involves the tight interaction of many processes. At dawn, the layer near the surface is generally saturated, and stabilized by precipitation late in the previous day, and by radiative cooling at night (see Betts *et al*., 2002). The surface sensible and latent heat fluxes are trapped initially in a shallow stable layer less than 400m deep, and so initially θ and q rise rapidly in a shallow growing mixed layer. This process is reasonably represented in the model, but only two hours after sunrise, model representation and reality separate. At the Abracos pasture site, a shallow cumulus layer deepens rapidly once the nocturnal BL is penetrated, since the atmosphere above 950 hPa is conditionally very unstable, and transports the large surface evaporation up and out of the subcloud layer. In the easterly wind regimes, mixed layer q even starts to fall around 1300-1400 UTC (0900-1000 LST) as a result of this upward transport of moisture into non-precipitating clouds (Figure 11). The developing cumulus grow deep enough to produce the first radar echoes about 1500 UTC (1100 LST), and the first showers often form near local noon. Organized convective bands typically take until around 1800 UTC (1400 LST) to develop in this Rondônia region (Silva Dias *et al*., 2002). The model convective parameterizations do not describe this growing cumulus BL stage at all well. In fact, as soon as the surface heating in the model breaks though the nocturnal BL about two hours after sunrise, the deep convective parameterization, "sees" the deep conditionally unstable atmosphere, calculates a convective cloud-top in the upper troposphere, and produces convective rain (see Figure 10a), computing a timescale for the process from a CAPE (convective available potential energy) closure. Although the shallow cloud parameterization (which has its own equilibrium closure, based on moist static energy balance in the sub-cloud layer in a single time-step) is activated intermittently, most

of the morning growing shallow cumulus BL phase is bypassed in the model. Calculating cloud-top, or the depth of the CBL, during this morning growth phase is a challenging problem in a numerical model, as the tropical atmosphere over Rondônia in the rainy season is so conditionally unstable from 900- 600 hPa. The reason is that, unless there is a strong inversion as in the trade winds, the depth of the CBL as it evolves, is determined by mixing or entrainment processes between the clouds and their surroundings. As yet, no suitable general formulation of this entrainment process has been found, which will give the depth of the growing CBL in the very unstable atmosphere of the tropics over land. It seems clear also that most large scale models, including the ECMWF model, are deficient in the way they separate convection and clouds into separate parameterizations. Rather than the continuum of convection seen in nature; in the model, the growing convective BL is broken into a dry convective process and a shallow cloud process; and furthermore shallow and deep convection are computed with two separate parameterizations with distinct closures.

The near-surface diurnal cycle of the thermodynamic variables and the surface fluxes (not shown) are influenced by the evaporation of falling precipitation, which occurs too early in the model. Cloud-base and near-surface temperature are lower than observed in the model in the early afternoon by about 1K and 20 hPa, These biases are however small by global model standards. Interestingly enough the model comes within ±2K of replicating the maximum afternoon θ_E observed of around 358K, although there is no evidence that the model represents well the convective downdraft process, which can be seen to bring low θ_E air into the sub-cloud layer. The daytime diurnal cycle of mixing ratio in the model is within ± 0.5 g kg^{-1} of observations, which is also good for the moist tropical BL, although the detailed differences seen between the composites are not reproduced. The model has a small high bias in evaporative fraction (not shown). One cause is that the early precipitation

in the morning fills the model surface water reservoir, which evaporates unimpeded by stomatal control.

5. CONCLUSIONS

This paper has reviewed the nature of the diurnal thermodynamic cycle over land using illustrations from high latitudes to the tropics. The coupling between different processes at the land surface is of fundamental importance, because in global models many processes are parameterized, and are poorly constrained by routine observational inputs. Yet the diurnal cycle is observed synoptically, so it is an excellent indicator of whether the surface processes are correctly modeled, and of course it is a key forecast product.

The first section showed how, given a similar net radiation budget at the surface at a grassland site, soil moisture controls evaporation (through its impact on stomatal resistance), and the diurnal cycles of temperature, and relative humidity. The pre-existing or residual BL above the nocturnal stable BL has a large impact of the details of the diurnal cycle as the morning ML grows. This was illustrated comparing 2 days over the boreal forest in spring, when a deep BL develops because very little water is available for evaporation. The fundamental link between resistance to evaporation and the diurnal cycles of RH and P_{LCL} distinguishes the land surface from the ocean surface, where the surface is saturated. A section on the diurnal cycle of CO_2 and its daytime vertical gradients was included to emphasize the importance of CO_2 as a climate variable, not only for its radiative significance, but because it is tightly coupled in the BL to water vapour.

A section was included discussing further the diurnal cycle over the boreal forest: the seasonal

cycle of the diurnal cycle, and the dependence of the diurnal cycle of P_{LCL} on surface water reservoirs. At high latitudes, the seasonal cycle of temperature is large, and soil freezing plays a major climatic role. In spring, water is not available for evaporation until the ground melts. A monotonic increase of the diurnal cycle of RH (decrease of LCL) was seen in northern Manitoba from April to October. Surface water stores, particularly in the moss layer, play an important role in surface evaporation in summer.

The comparisons between the ECMWF model and the Rondônia data illustrates the process of identifying model diurnal cycle errors and their causes. The model diurnal cycle of precipitation is clearly in error in the wet season over the southern Amazon, and the cause is the poor representation of the growth of the shallow cumulus boundary layer. Although the model diurnal cycle of the near-surface thermodynamics is quite close to that observed, it is being produced in the model by a different mix of boundary layer and surface processes, primarily more rainfall evaporation and less shallow cumulus convection than is observed. Consequently the model diurnal cycle most closely resembles the westerly wind regime in late February, when showers were more frequent. Data comparisons of this type can be used both to identify errors and to systematically improve and unify the model convective parameterizations, until they simulate reality more closely.

Acknowledgments. Alan Betts acknowledges support from the National Science Foundation under grant ATM-9988618, from NASA under grants NAG5-7377 and NAG5-8364.

References

Betts, A.K. (1982) Saturation Point Analysis of Moist Convective Overturning. *Journal of the Atmospheric Sciences* 39, 1484-1505.

Betts, A.K. (1997) 'The Parameterization of deep convection', Chapter 10 (pp 255-279) in "*The Physics and Parameterization of Moist Atmospheric Convection*, Ed. R. K. Smith, NATO ASI Series C: Vol. 505, Kluwer Academic Publishers, Dordrecht, 498pp.

Betts, A.K. (2000) Idealized model for equilibrium boundary layer over land. *Journal of Hydrometeorology* 1, 507-523.

Betts, A.K. and Ball, J.H. (1995) The FIFE surface diurnal cycle climate. *Journal of Geophysical Research* 100, 25679-25693.

Betts, A.K., Goulden, M.L. and Wofsy, S.C. (1999) Controls on evaporation in a boreal spruce forest. *Journal of Climate* 12, 1601-1618.

Betts, A.K., Ball, J.H. and McCaughey, J.H. (2001) Near-surface climate in the boreal forest. *Journal of Geophysical Research* 106, 33529-33542.

Betts, A.K., Fuentes, J. Garstang, M. and Ball, J.H. (2002) Surface diurnal cycle and Boundary Layer structure over Rondonia during the rainy season. *Journal of Geophysical Research* (in press).

Betts, A.K. and Jakob, C. (2002) Evaluation of the diurnal cycle of precipitation, surface thermodynamics and surface fluxes in the ECMWF model using LBA data. *Journal of Geophysical Research* (in press).

Gregory, D., Morcrette, J.-J., Jakob, C., Beljaars, A.C.M. and Stockdale, T. (2000) Revision of the convection, radiation and cloud schemes in the ECMWF model. *Quarterly Journal of the Royal Meteorological Society* 126, 1685-1710.

MacPherson, J.A. (1994) NRC Twin Otter operations in BOREAS 1994. *Report LTR-FR-129* from

Institute for Aerospace Research, National Research Council, Canada.

Jarvis, P.G., and Linder, S. (2000) Constraints to growth of boreal forests. *Nature* 405, 904-905.

Rickenbach, T. M., Ferreira, R.N., Halverson, J. and Silva Dias, M. A. F. (2002) Mesoscale properties of convection in western Amazonia in the context of large-scale wind regimes. *Journal of Geophysical Research* (in press).

Rouse, W.R. (2000) The energy and water balance of high latitude wetlands. *Global Change Biology* 6, 59-68.

Silva Dias, M.A.F., Rutledge, S., Kabat, P., Silva Dias, P.L., Nobre, C., Fisch, G., Dolman, A.J., Zipser, E., Garstang, M., Manzi, A., Fuentes, J.D., Rocha, H., Marengo, J., Plana-Fattori, A., Sá, L., Alvalá, R., Andreae, M.O., Artaxo, P., Gielow, R. and Gatti, L. (2002) Clouds and rain processes in a biosphere atmosphere interaction context in the Amazon Region. *Journal of Geophysical Research* (in press).

Van den Hurk, B.J.J.M., Viterbo, P., Beljaars, A.C.M. and Betts, A.K. (2000) Offline validation of the ERA40 surface scheme. ECMWF Technical Memo # 295. Available from ECMWF, Shinfield Park, Reading RG2 9AX, UK. 43pp.

Viterbo, P., Beljaars, A.C.M., Mahfouf, J.F., and Teixeira, J. (1999) The representation of soil moisture freezing and its impact on the stable boundary layer. *Quarterly Journal of the Royal Meteorological Society* 125, 2401-2426.

Table 1. Surface diurnal composites.

Composite Name	Days included [UTC]	Mean daily precipitation [mm]	
		Observed	ECMWF model
1. East 20-28	20-28	5.7	8.5
2. West 29-38	29-38	6.9	4.9
3. East 39-52	39-52	7.5	7.3
4. West 53-59	53-59	10.1	10.7
5. WET-8 days	20,24,30,31,38,42,44,48 (Afternoon rainband)	8.9	8.4
ALL DAYS	20-59	7.4	7.6

List of Figures

current ECMWF model .

Fig. 10b. As Fig. 10a for observed mean diurnal cycle of precipitation over Rondônia; an average of four raingage networks.

Fig. 11. Comparison of surface thermodynamic cycle in ECMWF model (left) with LBA pasture site (right).

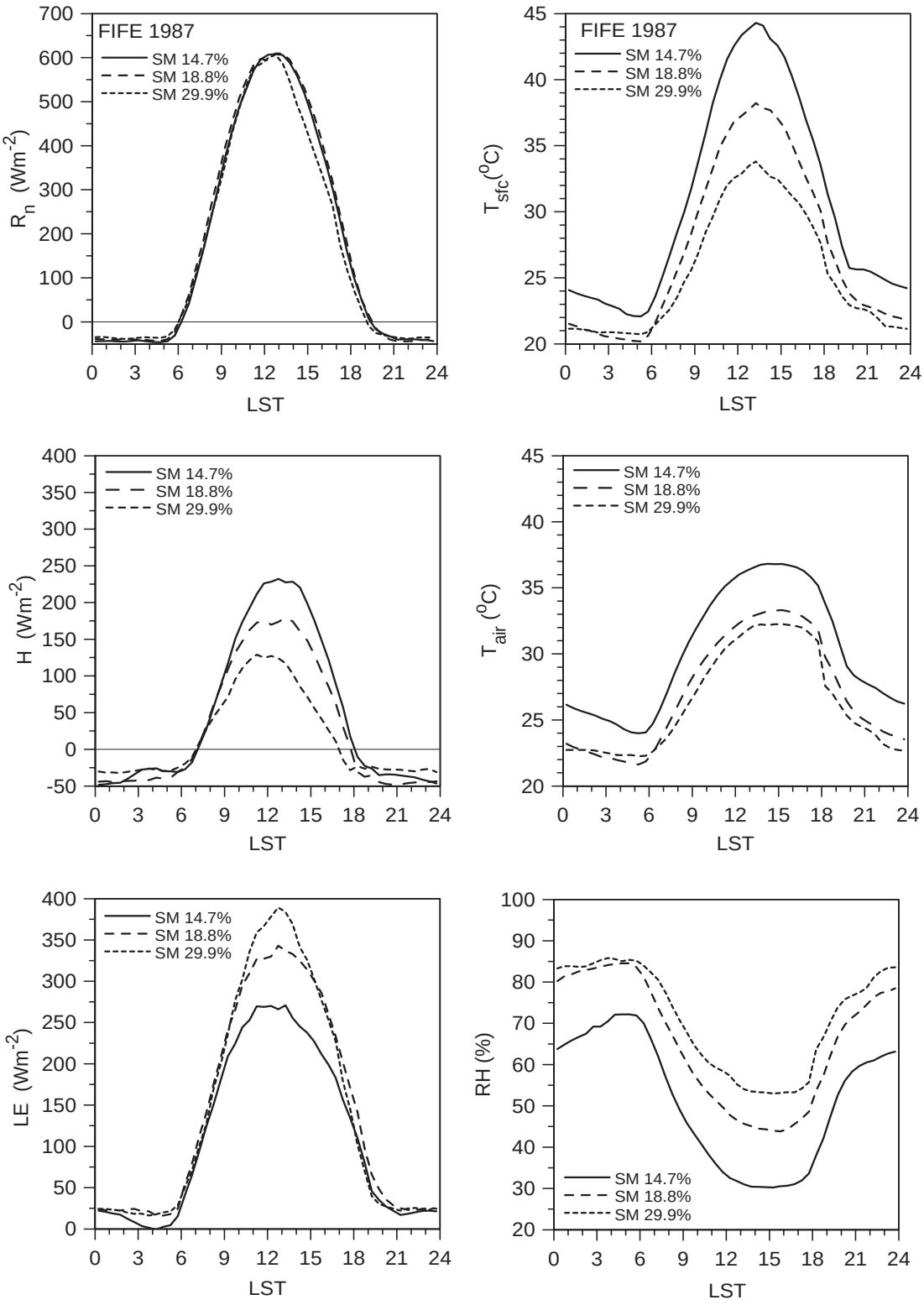

Fig. 1. Diurnal cycle of net radiation (R_n), sensible heat flux (H) and latent heat flux (LE) (left panels); surface temperature, air temperature and relative humidity (right panels), stratified by percent volumetric soil moisture in first 10cm of the soil.

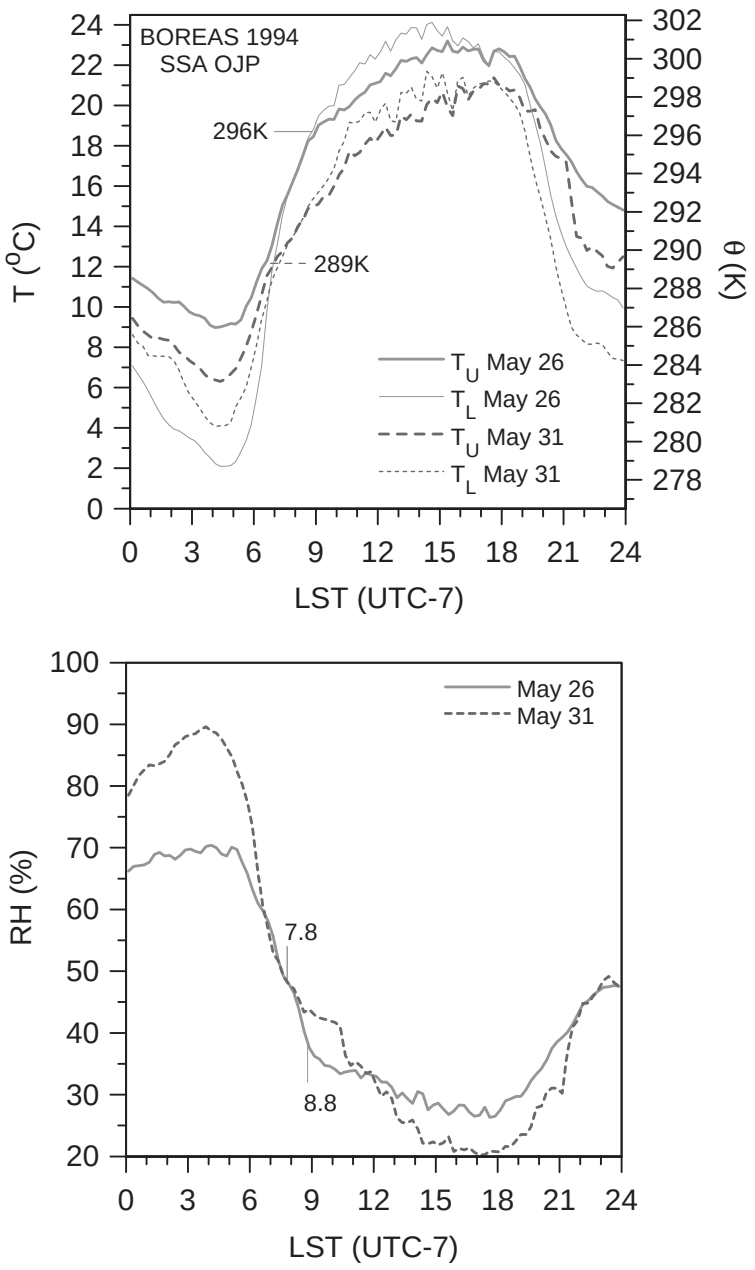

Fig. 2. Diurnal cycle of temperature, above and below a boreal forest canopy (upper panel), and of relative humidity above the canopy (lower panel) for two days in May, 1994.

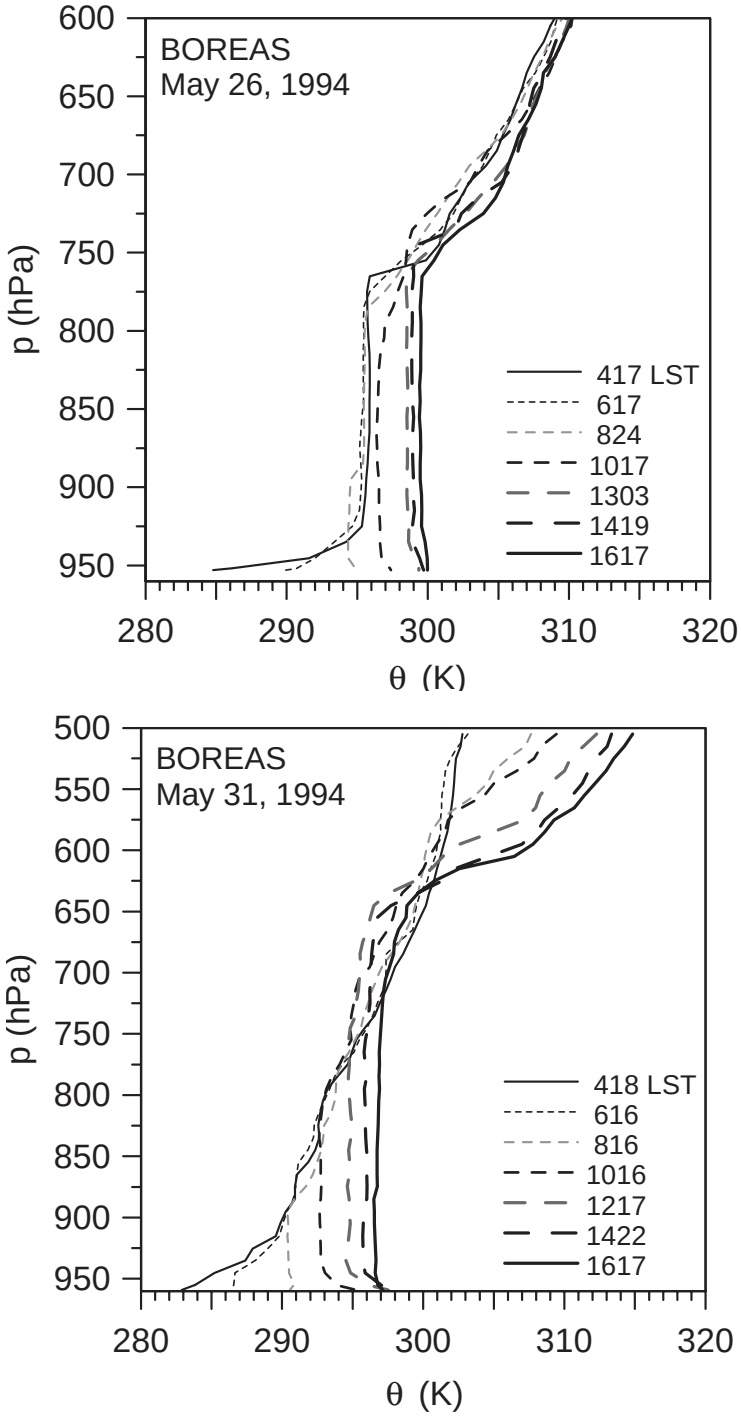

Fig. 3. Profiles of potential temperature in the lower troposphere on May 26 and 31.

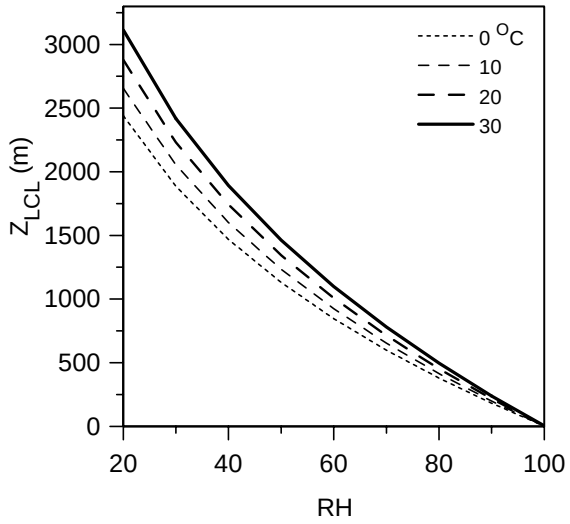

Fig. 4a.. Relation between height of LCL and RH as surface temperature varies. [Note independent of surface pressure]

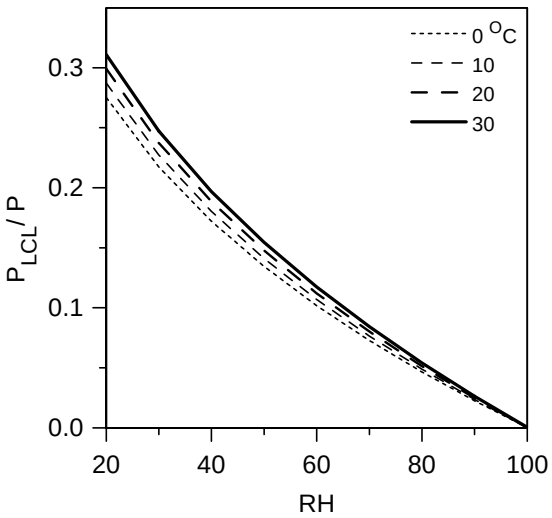

Fig.4b. As Fig. 4a for ratio of P_{LCL} to surface pressure p [Note dependence on T is weak]

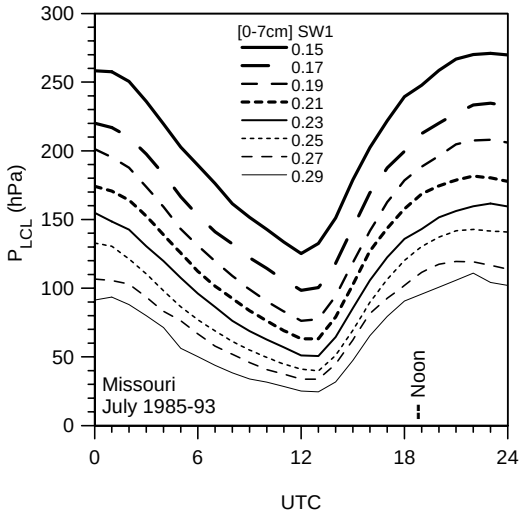

Fig. 5a. Mean diurnal cycle, stratified by soil moisture, for Missouri basin for July 1985-1993 from ERA-15. Local noon (near 1830 UTC) is marked.

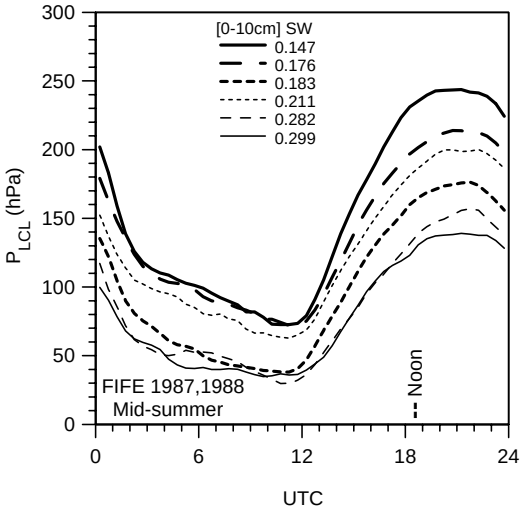

Fig 5b. As Fig. 5a for FIFE 1987 and 1988 mid-summer composites.

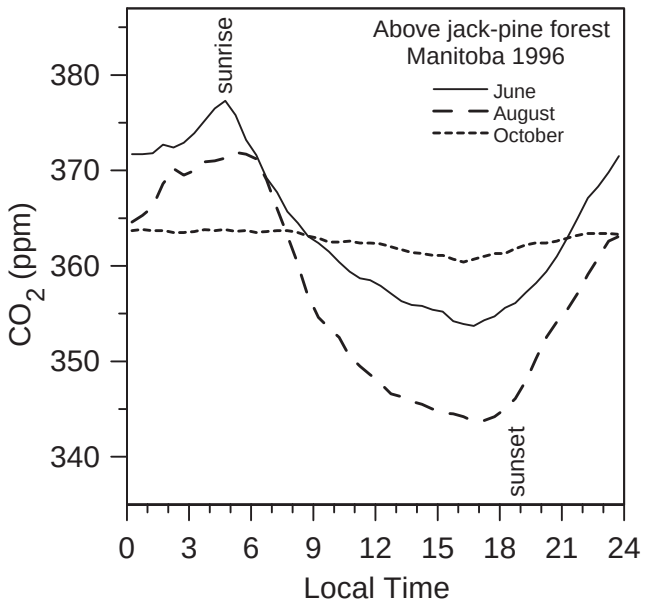

Fig. 6. Monthly mean diurnal cycle of CO_2 for June, August and October for a boreal jack-pine site.

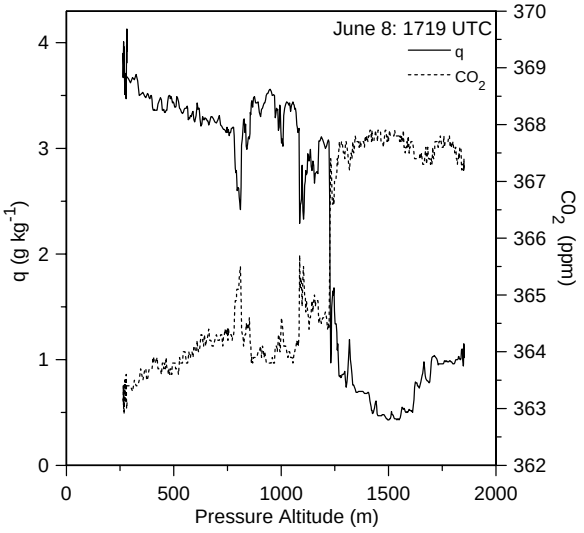

Fig. 7a. Profiles of mixing ratio, q, and CO_2 from surface to 1800m.

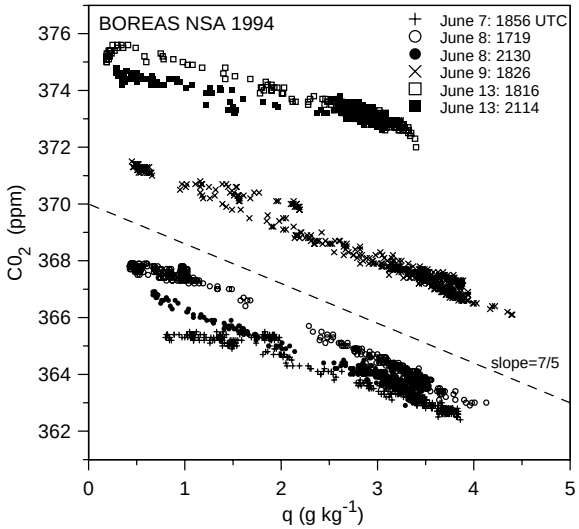

Fig. 7b. Six aircraft profiles through the boundary layer, showing strong coupling between q and CO_2 fluctuations.

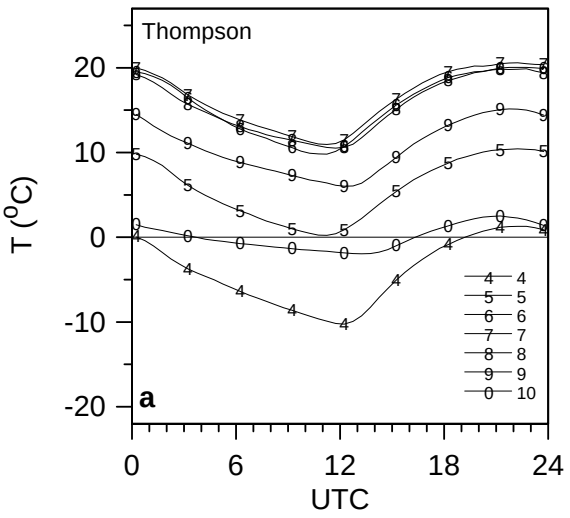

Fig. 8a. Diurnal cycle of above canopy temperature for Thompson.

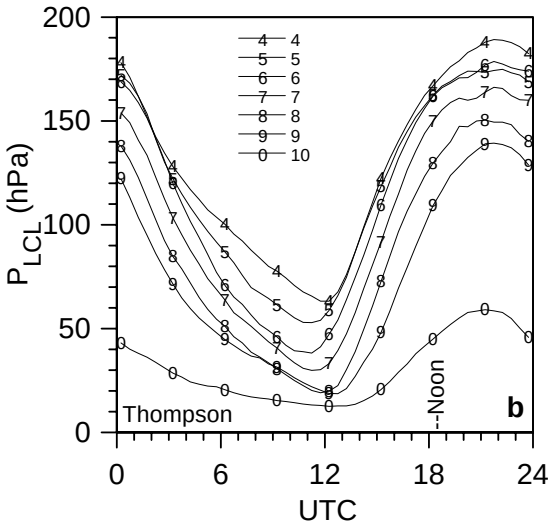

Fig. 8b. As Fig. 8a for P_{LCL} .

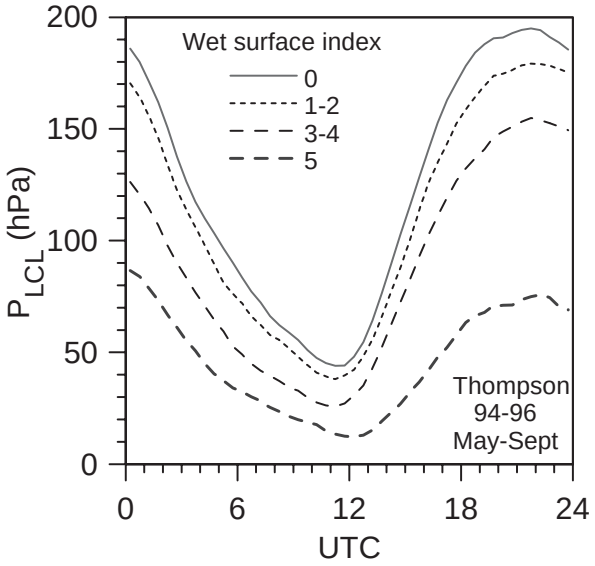

Fig. 9. Diurnal cycle of P_{LCL} for Thompson, MB, stratified by wet surface index.

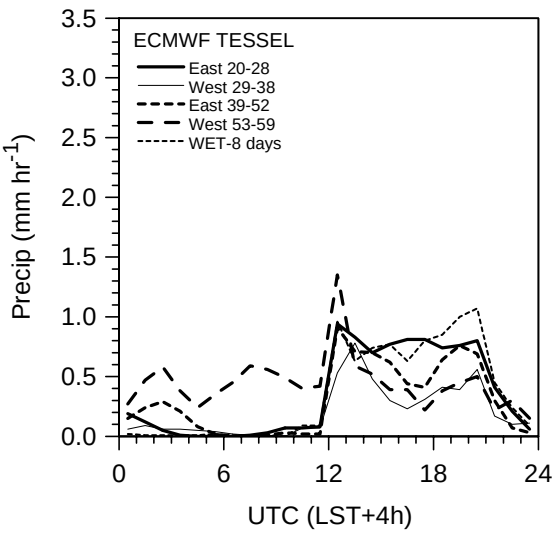

Fig. 10a. Mean diurnal cycle of precipitation over Rondônia for 5 convective classifications for current ECMWF model.

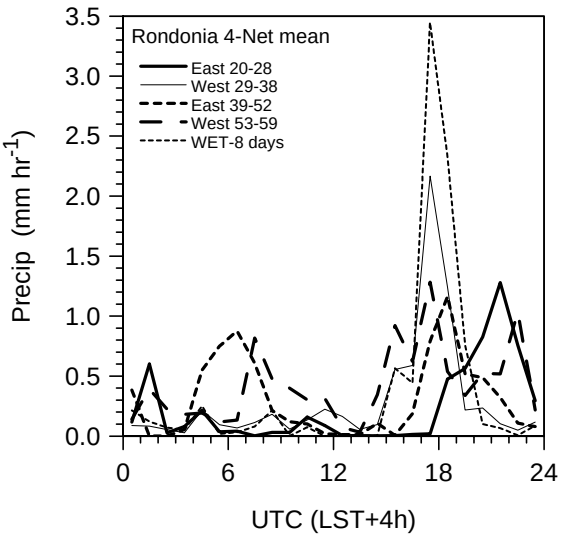

Fig. 10b. As Fig. 10a for observed mean diurnal cycle of precipitation over Rondônia; an average of four raingage networks.

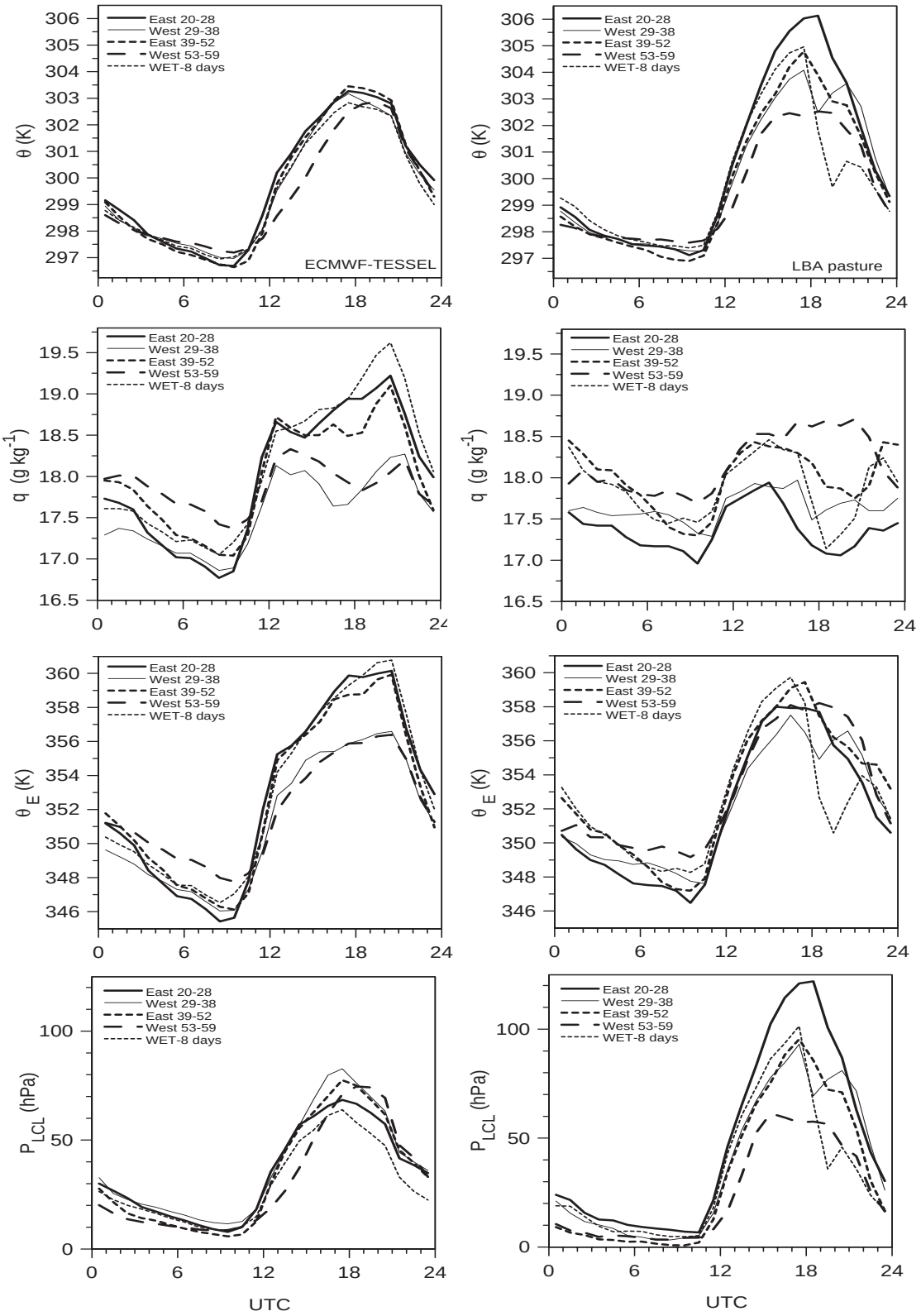

Fig. 11. Comparison of surface thermodynamic cycle in ECMWF model (left) with LBA pasture site (right).